Cathodoluminescence of defects in diamond films and particles grown by hot-filament chemical-vapor deposition

L. H. Robins, L. P. Cook, E. N. Farabaugh, and A. Feldman
Ceramics Division, Institute for Materials Science and Engineering, National Institute of Standards and Technology, Gaithersburg, Maryland 20899
(Received 28 November 1988)

Point defects, impurities, and defect-impurity complexes in diamond particles and polycrystalline films were investigated by cathodoluminescence (CL) imaging and spectroscopy in a scanning electron microscope. The diamond films and particles were grown by hot-filament methane-hydrogen chemical-vapor deposition at several different temperatures; the nominal deposition temperature (T_d) ranged from 600 to 850 °C. Electron-beam energies used to excite the CL were 10–30 keV. By comparing the CL spectra to spectra of known defects in natural and synthetic diamond, the following luminescence centers were identified: (a) 2.156-eV center (zero-phonon line observed at 2.15±0.01 eV) attributed to a nitrogen-vacancy complex; (b) 2.326-eV center (observed peak position at 2.32±0.01 eV), also thought to be a nitrogen-vacancy complex; (c) violet-emitting center (observed peak position at 2.82±0.01 eV), associated with dislocation line defects, whose atomic structure is uncertain; (d) 3.188-eV center (observed peak position at 3.189±0.001 eV), attributed to interstitial nitrogen or a nitrogen–(carbon-interstitial) complex; (e) isolated neutral vacancy (denoted the general radiation center) with principal zero-phonon line at 1.673 eV (observed peak position at 1.675±0.002 eV). The luminescence from each center displayed a different dependence on T_d and film morphology, as follows: (a) 2.156-eV center, maximum at $T_d = 600$ °C, corresponding to a cubic crystal-growth habit; (b) 2.326-eV center, similar to (a); (c) 2.82-eV center, maximum at $T_d = 750$ °C, octahedral crystal-growth habit; (d) 3.188-eV center, maximum at 650 °C, transition between cubic and octahedral crystal growth; (e) 1.673-eV center (neutral vacancy), observed only at 850 °C, relatively indistinct crystal-growth habit. CL from center (d) was induced by extended exposure to the electron beam. CL imaging of large (~10-μm) crystalline particles suggests that centers (a) and (c) are located primarily near {100} faces; the dislocation-related center (c) appears to be slightly more confined to near-surface regions than center (a).

I. INTRODUCTION

Following the recent discovery that particles and films of crystalline diamond can be grown on nondiamond substrates by low-pressure, energetically assisted, chemical-vapor deposition (CVD), there has been a rapid increase of interest in the growth and properties of these materials.[1,2] Among the reasons for this interest are the possible optical and electronic applications of CVD diamond,[3] which are expected to take advantage of desirable intrinsic properties, such as optical transparency over a wide spectral range and high carrier mobilities. Because the diamond films grown thus far by CVD are polycrystalline and highly defective, their properties differ in many respects from the intrinsic properties of perfect diamond crystals.

Relatively little characterization has yet been done of lattice defects and chemical impurities in CVD-grown diamond. The defects and impurities that have a strong influence on the optical and electronic properties are primarily those that possess electronic energy levels within the forbidden gap of the perfect crystal. By analogy to natural and high-pressure synthetic diamond, as well as to related materials such as silicon, the states of interest may include vacancy and self-interstitial point defects, line defects (dislocations), planar defects (stacking faults), substitutional and interstitial impurity atoms, and complexes composed of several simple defects or impurities. Many such states have been observed and characterized in diamond by optical spectroscopies such as optical absorption, luminescence,[4,5] and photoconductivity.[3] It should be possible to apply these techniques to CVD-grown diamond films.

Cathodoluminescence (CL), the optical emission arising from electronic recombination following excitation by an energetic electron beam,[6] has been one of the most successful techniques for characterizing defects and impurities in diamond. Typical electron-beam energies for CL excitation are 5–50 keV, well above the energy range of interband transitions in diamond[7] (5.5–30 eV); electron-hole pairs are generated as the primary electron beam undergoes inelastic collisions within the diamond crystal. In contrast, photoluminescence (PL) is typically excited in diamond[5] by light of photon energy below the band gap (5.5 eV), due to the lack of intense light sources further in the ultraviolet. CL is, in general, a less selective method of excitation than PL, and causes a greater variety of defects to luminesce.

When CL is excited by the electron beam of a scanning electron microscope (SEM), high-resolution imaging[6] of

the luminescent defects can be performed. The spatial resolution of the image, typically 0.1–0.5 μm, is determined by the spot size of the focused electron beam and by beam spreading inside the specimen. The wavelength of the emitted light does not limit the resolution because the image is that of the electron-beam–excitation region, not the region of optical emission.

There have been two previous CL studies of CVD-grown diamond. In the first study, CL spectra were measured in homoepitaxial diamond films grown on single-crystal natural diamond substrates by thermal CVD.[8] Spectra observed in films grown on {100} and {111} faces were compared, and changes in the CL resulting from chemical doping with nitrogen or boron were examined. Several narrow CL lines were observed, and attributed to nitrogen interstitials, vacancy and nitrogen-vacancy complexes, and silicon interstitials (which presumably originated from etching of the silica walls of the CVD reactor). Broad CL bands were attributed to dislocations and, in the boron-doped film, to donor-acceptor pairs. In the second study, diamond films[9] grown by microwave and magnetomicrowave plasma-enhanced CVD were characterized by CL imaging and spectroscopy. In the latter study, no narrow lines were observed; the CL was seen to consist of broad bands in the blue and green, attributed to deep-donor–to–acceptor recombination. Imaging showed that the CL arose primarily from the {100} crystal faces.

In the present work we describe the initial results of a study of luminescent defects in CVD-grown diamond films and the effect of deposition temperature on these defects. By comparing CL spectra in these films to the spectra of known defects in natural and synthetic diamond, several types of defects present in the films were identified. These include the following: (a) 2.156-eV center attributed to a nitrogen-vacancy complex;[10–15] (b) 2.326-eV center, also thought to be a nitrogen-vacancy complex;[8] (c) violet-emitting (2.82-eV) center associated with dislocation line defects;[16] (d) 3.188-eV center attributed to interstitial nitrogen or a nitrogen–(carbon-interstitial) complex;[17–19] (e) isolated neutral vacancy[4,5] [denoted the general radiation (GR) center] with principal zero-phonon line at 1.673 eV (observed peak position at 1.675±0.002 eV). (The spectroscopic identification of these optical centers in our specimens is explained in more detail in Sec. IV.) The majority of these defects were previously observed[8] in the study of films grown by homoepitaxial thermal CVD. CL was also observed in isolated diamond particles grown under similar deposition conditions. Scanning electron imaging of the dominant luminescent defects, performed in the isolated particles, showed that these defects are associated primarily with {100} crystallographic faces, and not with {111} faces, in agreement with the results of CL imaging[9] in diamond films grown by microwave-plasma-enhanced CVD.

II. EXPERIMENTAL PROCEDURE

The diamond films examined in this study were grown in a hot-filament methane-hydrogen chemical-vapor deposition system. Figure 1 shows a schematic diagram

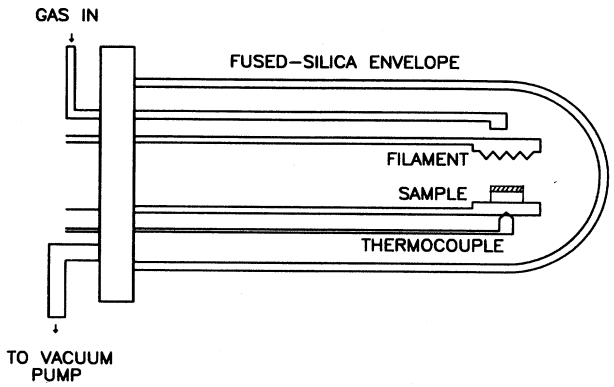

FIG. 1. Experimental apparatus for growth of diamond films by the hot-filament chemical-vapor-deposition method.

of the system, which was previously described[20] in more detail. Films were deposited on polished silicon single-crystal substrates cut at 5° off the (100) axis. [The substrates were cut at an angle to determine whether an off-axis substrate increases the diamond nucleation rate relative to an on-axis silicon (100) substrate; in our experiments, no difference was observed between nucleation on on-axis and off-axis substrates.] The deposition conditions for these films were gas mixture, 0.5% methane and 99.5% hydrogen; total gas-flow rate, 52 standard cubic centimeters per minute (sccm); deposition pressure, 5×10^3 Pa; filament material, tungsten; and filament temperature, approximately 1800 °C. The vacuum was maintained by a rotary mechanical pump; the base pressure in the deposition chamber was 20 Pa. Six specimens were prepared at deposition temperatures, T_d, of 600, 650, 700, 750, 800, and 850 °C. Growth at $T_d=550$ °C was also tried, but no film was deposited at that temperature. T_d was measured by a thermocouple in contact with the back surface of the substrate, away from the hot filament; thus, the actual temperature of the growing film may have been significantly higher than T_d because of radiation heating by the filament. The substrates were rubbed with diamond paste, and subsequently cleaned, to facilitate the growth of continuous films. Another deposition was carried out at 800 °C on a nonrubbed substrate in order to grow isolated diamond particles.

Cathodoluminescence was excited in the specimens by the electron beam of a scanning electron microscope (SEM). For the measurements of CL spectra, the electron-beam voltage was 20 kV, the beam current was 2.2×10^{-8} A, and the spot size on the specimen was estimated to be 0.5 μm. For CL imaging, smaller spot sizes were used to improve the image resolution. For the images produced at a beam voltage of 10 kV, the beam current was 1.9×10^{-9} A and the estimated spot size was 0.14 μm; at 20 kV, the beam current was 1.8×10^{-9} A and the spot size was 0.11 μm; and at 30 kV, the beam current was 1.3×10^{-9} A and the spot size was 0.08 μm. (The alignment of the electron optics in the CL experiments was different from the alignment used to measure the electron spot sizes; therefore, the estimates for the

spot sizes may be inaccurate.)

The luminescence from the specimen was collimated by a fused-silica lens and transmitted through a fused-silica window. For CL imaging the luminescence was detected by a photomultiplier tube (PMT) and the detector signal was then sent to the image-production system of the SEM. Spectrally resolved CL imaging was accomplished by placing optical interference filters in front of the PMT, which had an S20 spectral response. The interference filters had center wavelengths from 400 to 850 nm and bandwidths of 40 nm.

For CL spectroscopy the luminescence was focused onto the entrance slit of a 0.18-m monochromator by a second silica lens. The spectrally dispersed light in the exit plane of the monochromator was detected by an optical multichannel analyzer, consisting of a microchannel plate intensifier and 700-element silicon photodiode array. Spectral data from the multichannel analyzer were transferred to a computer for storage, display, and further analysis. A diagram of the CL spectroscopy experiment is shown in Fig. 2.

The CL photon-energy range accessible with the above setup was approximately 1.4–3.5 eV. Wavelength calibration of the spectrograph to an accuracy of 0.1 nm was accomplished with a set of spectral line lamps. A 1000-W quartz-halogen lamp, of the type used as a National Bureau of Standards (NBS) [now National Institute of Standards and Technology (NIST)] standard of spectral irradiance, was used to measure the spectral response of the spectrograph. The latter calibration allowed the CL spectra to be normalized in units of photons per eV incident on the spectrometer entrance slit. This normalization did not take into account the response function of the optics external to the spectrometer, which should not vary appreciably in the spectral range of interest. The chromatic aberration of the lenses, in conjunction with the narrowness of the spectrometer entrance slit (50 μm), did, however, have a noticeable effect on the shape of the observed spectrum. The effects of chromatic aberration appeared to be minimized by selection of an on-axis light path through the final lens and entrance slit. Care was therefore taken to maintain the on-axis optical alignment. To completely eliminate chromatic aberration, conversion to an all-reflecting optical system would be necessary, as planned for future experiments.

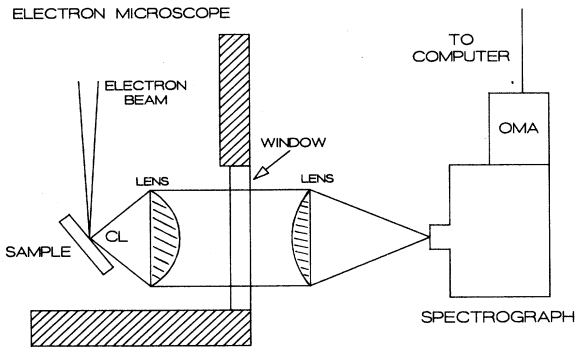

FIG. 2. Experimental apparatus for measurement of cathodoluminescence spectra excited in the scanning electron microscope. (For CL imaging, the second lens is replaced by a photomultiplier tube, and the photomultiplier output is connected to the image analysis electronics of the SEM.)

III. RESULTS

A. Cathodoluminescence spectroscopy

The spectra of the CL observed in each of the seven specimens are plotted in Fig. 3. The vertical scale of each spectrum in Fig. 3 was adjusted to best display the spec-

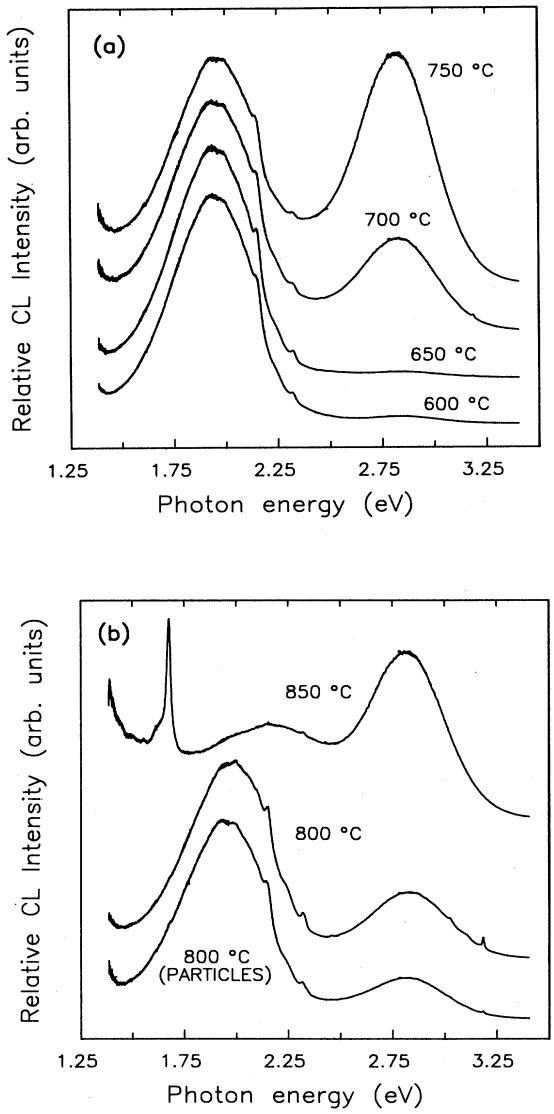

FIG. 3. CL spectra in hot-filament CVD diamond films grown at different deposition temperatures. Electron-beam energy is 20 keV. Spectra are corrected for spectrometer and detector response. (a) Films grown at deposition temperatures (T_d) of 600, 650, 700, and 750 °C. (b) Isolated particles grown at $T_d = 800$ °C and films grown at $T_d = 800$ and 850 °C.

tral features; hence they were not scaled uniformly. The relative intensities in each specimen of the main spectral peaks are shown in Fig. 4. The similarity between the CL spectrum of the isolated particles and the spectrum of the film grown at 800 °C [see Fig. 3(b)] suggests that the dominant luminescent defects in the isolated particles are virtually identical, in structure and concentration, to those in the film.

It is clear that the spectra shown in Fig. 3 are composed of several components, presumably arising from different types of defects. Two broad components are dominant. First, there is a violet component that is a very broad, symmetric, approximately Gaussian line with a peak energy of 2.82±0.01 eV and full width at half maximum (FWHM) of 0.42 eV. Second, there is a red-to-yellow component with an irregular, asymmetric line shape. The main features of the red-to-yellow component are a narrow peak or shoulder at 2.15±0.01 eV and a broad peak extending from 1.92 to 2.00 eV. The edges of the broad peak, at 1.92 and 2.00 eV, are narrow compared to its width. The intensity ratio of different spectral features within the red-to-yellow [(1.8–2.2)-eV] region remains constant from one specimen to another, suggesting that these features arise from the same type of defect in each specimen. (This interpretation is confirmed by comparison with CL spectra in non-CVD-grown diamond specimens, as discussed below.) Another common feature of the CL spectra is an apparent increase in intensity with decreasing photon energy at the lowest photon energies (~1.4 eV). This may be an artifact due to systematic experimental problems such as the incomplete rejection of light outside the selected wavelength interval by the monochromator, and the much lower sensitivity of the detector to 1.4-eV photons than to higher-energy photons.

The dependence of the relative intensity of the broad violet and red-to-yellow components on deposition temperature is plotted in Fig. 4. The violet peak is most intense in the specimen grown in the middle of the temperature range, at 750 °C, and decreases toward each end of the temperature range. The red-to-yellow peak is most intense in the specimen grown at the lowest temperature, 600 °C, and decreases with increasing deposition temperature.

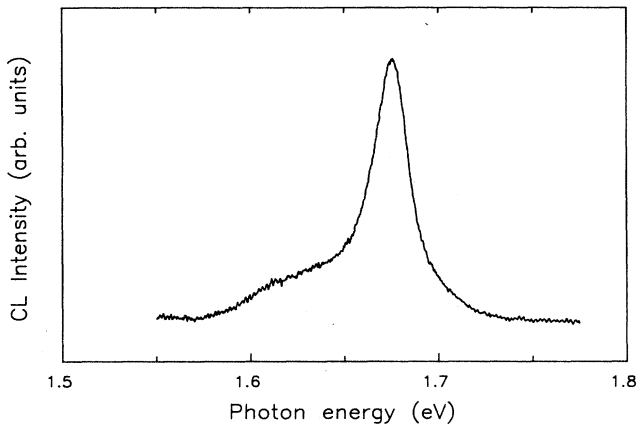

FIG. 5. CL spectrum of (1.675±0.002)-eV line in film grown at $T_d = 850$ °C, attributed to neutral vacancy, after subtraction of broad background component. Electron-beam energy is 20 keV.

In addition to the two dominant components, a weak line at 2.32±0.01 eV was observed in all specimens. A narrow line at 3.189±0.001 eV was observed in several specimens. Furthermore, an intense narrow line with a peak energy of 1.675±0.002 eV and FWHM of 0.025 eV was observed in the specimen grown at 850 °C, but was completely absent from all the specimens grown at lower temperatures. The (1.675±0.002)-eV line is plotted on an expanded energy scale, with background subtraction, in Fig. 5; it can be seen that there is a broad shoulder on

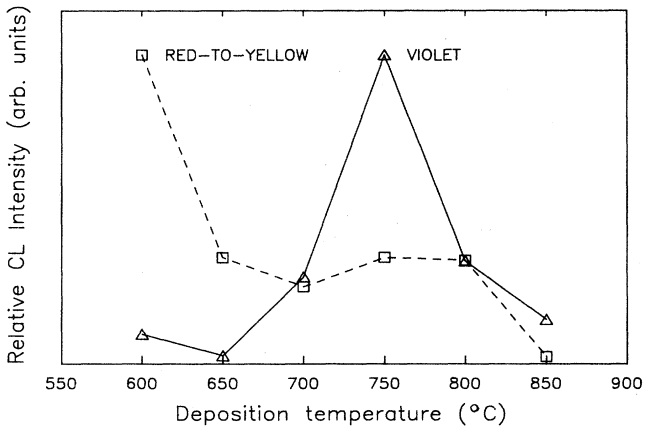

FIG. 4. Relative intensity of principal spectral components of CL as a function of deposition temperature (T_d). Squares: intensity of broad red-to-yellow component, measured at 1.92 eV. Triangles: intensity of broad violet component, measured at 2.82 eV. Data points are connected by lines to guide the eye.

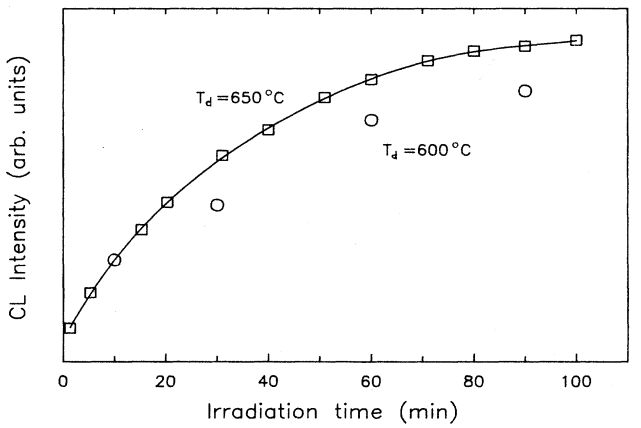

FIG. 6. Relative intensity of (3.189±0.001)-eV component as function of exposure time to electron-beam irradiation. Squares: film grown at $T_d = 650$ °C. Smooth curve is drawn to guide the eye. Circles: film grown at $T_d = 600$ °C. Electron-beam energy is 20 keV.

the low-energy side of the main peak.

The narrow line at 3.189±0.001 eV, which was seen in several specimens, but was especially strong in the specimen grown at 650 °C, displayed a noticeable increase in intensity after extended irradiation by the electron beam. Measurement of the dependence of the intensity on irradiation time, beginning at the time that the electron beam was moved to a fresh region of the specimen, suggests that the intensity approaches zero at the initial time; i.e., this luminescence is emitted only after exposure to the electron beam. The dependence of the CL signal on irradiation time is plotted in Fig. 6. The intensity increases rapidly at first, but then appears to saturate; the intensity reaches half of its saturation value 30 min after the onset of irradiation. For the $T_d = 600$ °C specimen, the dependence of the CL signal on irradiation time is similar to that of the 650 °C specimen, but the saturation intensity is smaller by a factor of ~20. After saturation intensity has been reached, the intensity remains at the saturated value when the electron beam is switched off for 30 min and then switched on again. This observation suggests that the change induced by the electron beam is irreversible at room temperature; possible annealing of the electron irradiation effect at higher temperature has not yet been investigated.

When the (3.189±0.001)-eV line is saturated, several satellite lines at lower energy also become apparent. These features of the 3.189-eV spectrum are superimposed on the spectrum of the broad violet (2.82-eV) component. The latter component decreases only slightly with irradiation. The broad violet component can thus be eliminated through the subtraction of spectra recorded at long and short irradiation times. The spectrum obtained by performing such a subtraction is shown in Fig. 7. We find that the principal line at 3.189±0.001 eV has a FWHM of 0.011 eV, and there are at least four satellite lines, which are broader and less intense than the principal line. The satellite lines are discussed later in the manuscript.

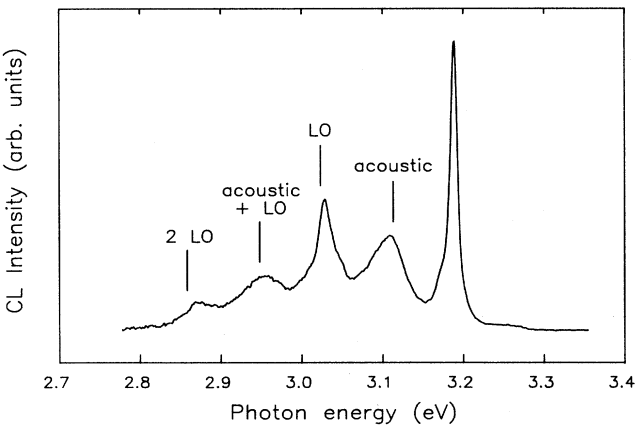

FIG. 7. Spectrum of (3.189±0.001)-eV component in $T_d = 650$ °C film, including principal (zero-phonon) and satellite lines, obtained by subtraction of spectra recorded after long (100 min) and short (1 min) electron-beam–irradiation times. Sidebands produced by coupling to 0.075-eV acoustic phonon and 0.165-eV longitudinal-optical (LO) phonon are labeled by vertical lines.

The spectral line shapes, and the relative intensities of all the various components in a particular specimen, do not vary noticeably with electron-beam energies of 10, 20, or 30 keV. Also, when the electron beam is moved from one area to another on the same specimen, the line shapes and relative intensities do not vary, except for the irradiation-induced component shown in Fig. 7. The distribution of luminescent defects in a particular specimen thus appears to be homogeneous on a scale of 50 μm or greater (50 μm is the longest dimension of the region traversed by rastering of the electron beam).

B. Crystal morphology

The morphology and crystal-growth habit of the specimens were examined by secondary-electron imaging in the scanning electron microscope, as shown in Fig. 8. Some empirical correlations may be made between variations in morphology with deposition temperature[20] and changes in the CL spectra (see Fig. 3). At 600 °C the growth habit of the crystal grains is predominantly cubic and cubo-octahedral, revealing many square {100} faces with smooth surfaces. A transition to an octahedral growth habit begins at 650 °C, and the grains are predominantly octahedral at 700, 750, and 800 °C. Well-defined triangular {111} faces with noticeable growth spirals are seen at 750 °C. In the CL the red-to-yellow component is most intense at 600 °C, where the growth habit is primarily cubic, while the broad violet component is most intense from 700 to 800 °C, where the growth habit is octahedral (see Fig. 4). From 750 to 850 °C more changes occur in the morphology; the growth spirals evolve into ledges and steps, secondary nucleation becomes important (small particles grow between the large grains), and the geometry of the large grains is less regular. At 850 °C there is pronounced secondary nucleation of particles with an amorphous appearance, almost completely covering the faces of the larger grains. All of the specimens, including the $T_d = 850$ °C specimen, produced a polycrystalline diamond x-ray-diffraction pattern. Both of the broad components of the CL decrease markedly with deposition temperature from 750 to 850 °C (see Fig. 4). The narrow-line CL spectra also appear to be correlated with particular morphologies. Although the irradiation-induced component (Fig. 7) occurs in several specimens, it is most intense in the 650- °C specimen, which appears to represent the transition between cubic and octahedral growth habits. The (1.675±0.002)-eV line is observed only in the 850- °C specimen, in which the crystalline diamond morphology is the most poorly defined and the intensity of the broad components of the CL is lowest. The (2.32±0.01)-eV line is observed in all specimens and behaves similarly to the broad red-to-yellow component.

C. Cathodoluminescence imaging

The distribution of luminescent defects was investigated by CL imaging of the isolated particles. While the CL

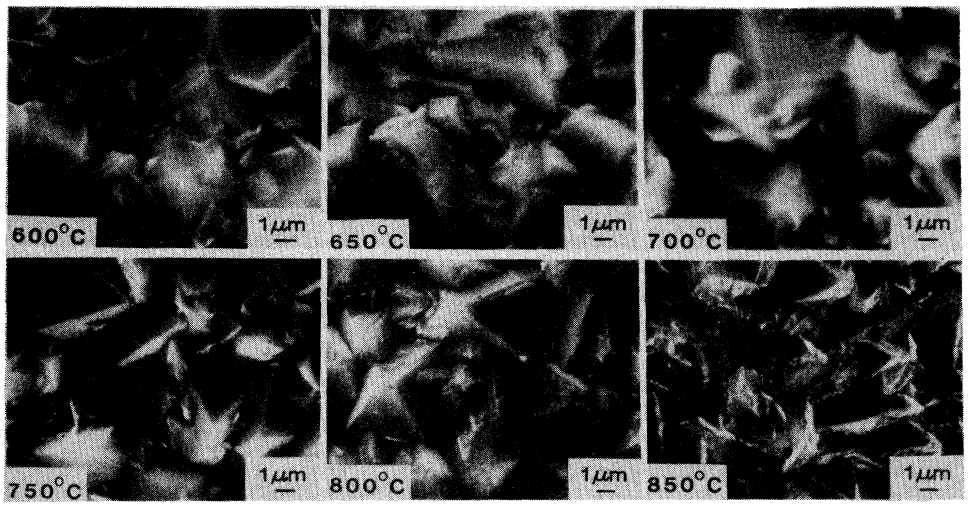

FIG. 8. Secondary-electron images of CVD diamond films, grown at six different deposition temperatures between 600 and 850 °C, obtained in scanning electron microscope at electron-beam energy of 20 keV.

spectrum of the particles consists of the same components as the spectra of the films [see Fig. 3(b)], the spatial separation and the relatively large size (~ 10 μm) of the particles facilitate the interpretation of the CL images, which have poorer spatial resolution than the SEM images. Three different CL images of a single spatial region, obtained, respectively, at electron-beam energies of 10, 20, and 30 keV, are shown in Fig. 9. A secondary-electron image and a backscattered electron image of the same region, both obtained at 20 keV, are shown in Fig. 10. The detector has the same orientation relative to the specimen for the CL, secondary-electron, and backscattered-electron images. It can be seen that the luminescence arises primarily from smooth-surfaced square or rectangular faces, which represent {100} crystal growth planes or possibly, in some cases, {110} planes. Several crystals in the selected area have a cubo-octahedral growth habit, and the square faces of these

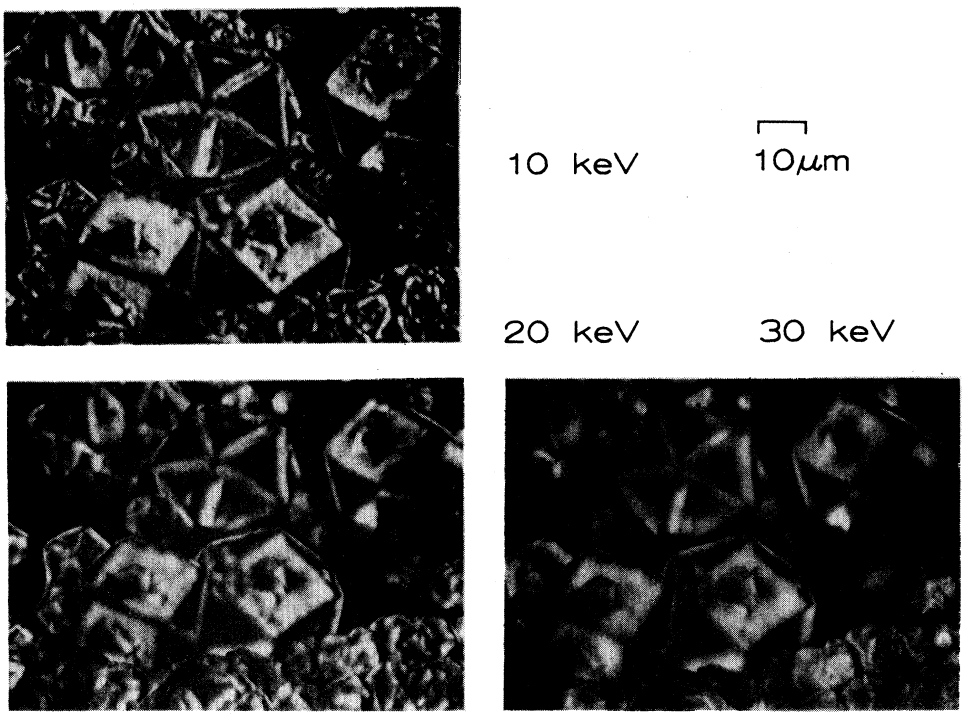

FIG. 9. CL images of isolated diamond particles, grown at 800 °C, obtained at electron-beam energies of 10, 20, and 30 keV.

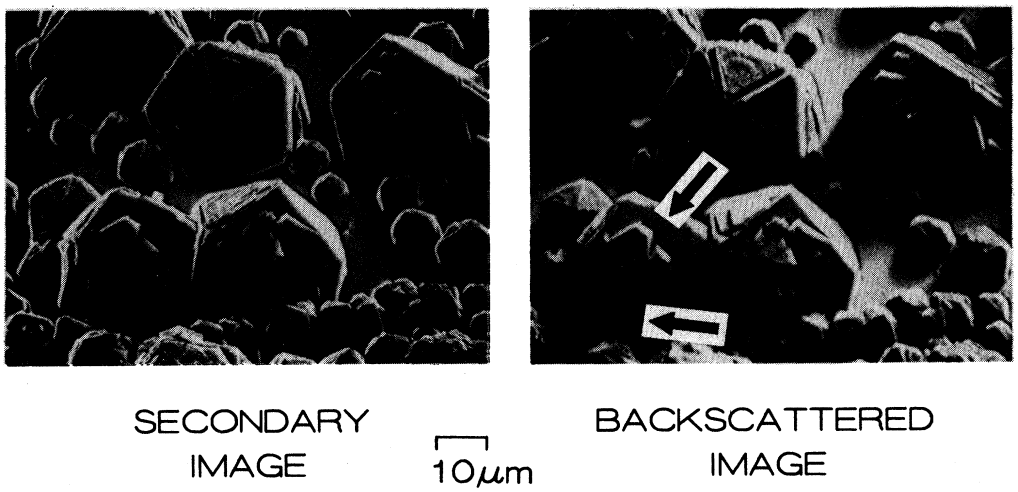

FIG. 10. Secondary-electron and backscattered-electron images of isolated particles; images of same spatial region as in Fig. 9; electron-beam energy is 20 keV.

crystals luminesce while the triangular faces do not. One crystal has a twinned icosahedral growth habit, which is often seen in CVD-grown diamond. The faces of the latter crystal are primarily triangular, but square or rectangular faces are visible as V-shaped grooves between the triangular faces. Luminescence in this crystal arises principally from the grooves, which causes the CL image of this crystal to have a starlike appearance.

Strong shadowing effects occur in the backscattered-electron image (Fig. 10), which is predominantly due to line-of-sight electrons impinging on the detector. Notice that in one crystal, located toward the lower left, a pair of adjacent square faces is visible (indicated by arrows in Fig. 10); one of these faces is deeply shadowed in the backscattered-electron image, while the other is illuminated. In the CL image, on the other hand, both faces are illuminated (see Fig. 9). As this example shows, the interpretation of the CL image is more complicated than the interpretation of the backscattered image, because luminescence originating near one crystal surface can propagate through the interior and exit through a surface with a different orientation.

The effective penetration depth of the electron beam[6] is approximately 0.9 μm at 10 keV, 2.9 μm at 20 keV, and 5.6 μm at 30 keV. Because of beam-spreading effects, the shape of the volume excited by the electron beam is approximately spherical. Excitation is thus confined to a near-surface layer at 10 keV, while virtually the entire volume of each crystal is excited at 30 keV. A comparison of the images obtained at 10, 20, and 30 keV (Fig. 9)

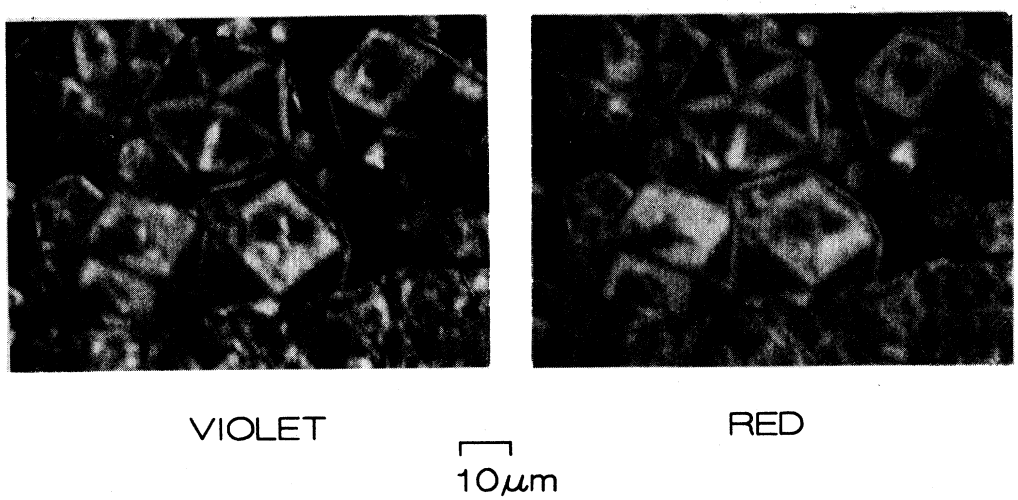

FIG. 11. Spectrally resolved CL images of isolated particles: broad violet component, 2.63–2.88 eV; broad red-to-yellow component, 1.85–1.97 eV; images of same spatial region as in Fig. 9; electron-beam energy is 20 keV.

shows that many details of the surface geometry which are resolved at the lowest electron-beam energy (10 keV) become increasingly diffuse at the higher energies. On the other hand, the distinction between luminescent square faces and dark triangular faces is fairly clear, even in the 30-keV image, suggesting that the luminescence arises primarily from a near-surface region even when the entire volume is excited. Notice also that boundaries between the crystals and the nonluminescent substrate surface remain sharp at 10, 20, and 30 keV.

Images of the two major components of the CL spectrum, obtained at 20 keV, are shown in Fig. 11. For ease of comparison, the same spatial region is imaged in Figs. 9–11. The spectral ranges of the images in Fig. 11 are, firstly, 2.63–2.88 eV, corresponding to the peak of the broad violet component, and, secondly, 1.85–1.97 eV, corresponding to the peak of the broad red-to-yellow component. These images have poor signal-to-noise ratio because of the reduction in luminescence intensity caused by the spectral selection process. The two spectrally resolved images are very similar to each other and to the unresolved images in Fig. 9. There is a difference which is most apparent in the interior of the square faces. Details of the surface geometry are better resolved in the image of the violet CL than in the image of the red-to-yellow CL. The difference between the two images suggests that the defects responsible for the violet CL are distributed closer to the surface, on average, than the defects responsible for the red-to-yellow CL. Because the difference between the red-to-yellow and violet images is subtle, more work is needed to confirm this interpretation.

IV. DISCUSSION

From the spectroscopic data, Figs. 3–7, at least five independent spectral components have been identified: (a) the broad, structured red-to-yellow component, with a plateau from 1.92 to 2.0 eV and shoulder at 2.15 eV; (b) the weak line at 2.32±0.01 eV; (c) the symmetric violet component centered at 2.82±0.01 eV; (d) the irradiation-induced component with its principal line at 3.189±0.001 eV; (e) the narrow line at 1.675±0.002 eV. It is clear that these components arise from distinct types of defects because their relative intensities vary with deposition temperature, and, in the case of (d), with electron-beam–exposure time. Considerable information about the nature of the luminescence defects can be obtained by comparing our results to previous work on CL spectra in diamond. The progress made in identifying spectral features (a)–(e) is summarized as follows.

Feature (a). Very similar spectra have been observed in polycrystalline diamond compacts that were fabricated by sintering synthetic diamond powder together with a metal binder.[10] In Fig. 12, CL spectra (from Ref. 10) of sintered diamond compacts with average grain sizes of 75, 25, and 10 μm are compared to the red-to-yellow spectral component in our CVD-grown films. The red-to-yellow component is identified as a vibronic spectrum[11] with zero-phonon line at 2.156 eV and dominant electron-phonon coupling to an acoustic-mode phonon at 0.075 eV and an optic-mode phonon at 0.16 eV. Residual stresses in the CVD films and in the sintered compacts are expected to increase with decreasing grain size, causing significant broadening of the vibronic structure. The shoulder at 2.15±0.01 eV in the strain-broadened spectrum corresponds to the zero-phonon line, the edge at ~2.00 eV corresponds to the optical-phonon sideband, and the edge at ~1.92 eV corresponds to the optical-plus acoustic-phonon sideband. From the broadening of the zero-phonon line, the average residual stress in the sintered diamond compacts was estimated to be 2.6 GPa for the 25-μm compact and 3.2 GPa for the 10-μm compact.[10] The line shape in the CVD-grown films is very similar to the line shape observed in these two compacts, suggesting that the residual stress in the CVD-grown films is also of the order of 3 GPa. Among the CVD-grown specimens, there is no significant difference between the line shape in the continuous polycrystalline films and in the specimen containing isolated particles (see Fig. 3), suggesting that interactions between distinct crystalline grains do not contribute significantly to the total internal stress.

The 2.156-eV center recently has been shown, by several independent experiments, to contain a single ni-

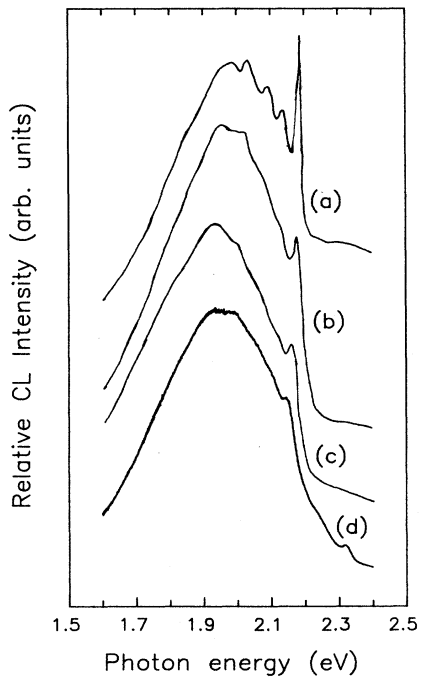

FIG. 12. Line shape of 2.156-eV vibronic spectrum (broad red-to-yellow component) in polycrystalline diamond specimens (Ref. 10): (a) sintered synthetic diamond compact, grain size 75 μm; (b) sintered compact, 25 μm; (c) sintered compact, 10 μm; (d) hot-filament CVD-grown films, average of data from five specimens with deposition temperature T_d between 600 and 800 °C, grain size 2–5 μm.

trogen atom. In homoepitaxial diamond films grown by thermal CVD,[8] the intensity of the 2.156-eV CL was significantly enhanced by doping with nitrogen during growth. In type-II*a* natural diamonds, the 2.156-eV center was produced by ion implantation with nitrogen, but not by ion implantation with any of 22 other elements, and, further, the intensity of the 2.156-eV CL band scaled linearly with nitrogen-ion dose.[12] (The classification of natural diamonds as type I*a*, I*b*, II*a*, or II*b*, according to their impurity content and resulting optical properties, is discussed in Ref. 4.) The observation of isotope shifts in ^{15}N-doped synthetic diamonds provided additional evidence for the nitrogen impurity nature of the center.[13] Earlier, uniaxial-stress experiments[14,15] demonstrated that the 2.156-eV center has trigonal symmetry, and suggested, because of the large magnitude of the stress splittings, that it may be vacancy related. A nearest-neighbor nitrogen-vacancy complex with a {111} symmetry axis is thus a plausible model for the center and seems to be consistent with all experimental results.

Feature (b). A CL line at 2.326 eV was observed in the thermal-CVD-grown homoepitaxial diamond films.[8] This line, similarly to the 2.156-eV line, was enhanced by doping with nitrogen during growth of the homoepitaxial films. Like the 2.156-eV line, the 2.326-eV line was observed to be significantly broader in the CVD-grown films than in single crystals, suggesting the large stress-splitting effect typical of vacancy-related centers in diamond. The 2.326-eV center may thus be a nitrogen-vacancy complex distinct from the 2.156-eV center.

Feature (c). Violet CL arising from dislocations in type-II*b* natural diamonds[16] was observed to have a symmetric line shape with a peak position of 2.83 eV and FWHM of 0.416 eV; the peak position and width are identical, within experimental uncertainty, to those of feature (c) in our CVD-grown films. (The peak position of the CL observed in Ref. 16 is stated to be 435 nm, or 2.85 eV. However, a conversion of units from photons emitted per unit wavelength, as in Ref. 16, to photons emitted per unit energy, as in the present work, causes the peak energy to shift down to 2.83 eV.) A broad violet component peaked near 2.8 eV was also observed in the sintered diamond compacts,[10] which have been shown to contain a high density of dislocations.[21] The atomic structure of the luminescence centers localized on the dislocations is not known, although a quasi-one-dimensional donor-acceptor pair has been proposed as the most plausible model. The dislocation CL in large natural crystals has been observed to be linearly polarized along the dislocation direction,[16] but no polarization effects were observed in CL imaging of our CVD-grown films.

A broad luminescence band in the green-to-violet region, denoted band-*A* luminescence, has been observed in many natural and synthetic diamonds.[5] The linewidth is of the order of 0.8 eV, and the peak may occur anywhere from 2.2 to 3.1 eV, depending on the impurity content of the particular specimen. The band-*A* luminescence is thought to arise from deep donor-acceptor pairs. The violet CL component in our CVD diamond films has a much closer resemblance to the dislocation-related violet luminescence than to the band-*A* luminescence described in the literature. In a recent CL study of diamond films grown by microwave-plasma-assisted CVD, the CL spectra were, however, found to be dominated by band-*A* emission in the blue and green,[9] with peak energies between 2.45 and 2.8 eV and a linewidth of 0.55 eV. It thus appears that both the dislocation-related violet luminescence centers and the band-*A* luminescence centers may occur in CVD-grown diamond. Because both spectra are broad and featureless, and their energy ranges overlap to a large extent, they can be difficult to distinguish, especially when both centers are present in the same specimen. It is also not clear to what extent the atomic structures of the two centers differ. If the deep donor-acceptor–pair model is the correct model for both, then the dislocation-related centers might be correctly described as a subset of the band-*A* centers in which the donor-acceptor pairs are localized near dislocations.

Feature (d). A vibronic CL spectrum with a zero-phonon line at 3.188 eV has been observed in many natural and synthetic diamonds.[17] The dominant electron-phonon coupling is to an acoustic phonon at 0.075 eV and the zone-center longitudinal-optical (LO) phonon at 0.165 eV. The following phonon bands are indicated by arrows in Fig. 7: the acoustic-phonon sideband at 3.113 eV, the LO-phonon sideband at 3.023 eV, the acoustic-plus-LO-phonon sideband at 2.948 eV, and, finally, the two–LO-phonon sideband at 2.858 eV. The 3.188-eV center, like the 2.156-eV center, has been shown to contain a single nitrogen atom by CL studies of natural diamond which was ion implanted with nitrogen and other impurities,[12] and also by CL studies of isotopic substitution in synthetic diamond.[18,19] (In the isotopic substitution experiment, diamond was synthesized from ^{13}C; the nitrogen-containing nature of the 3.188-eV center was revealed by its coupling to a local C—N stretching mode that shifted less with carbon-isotope substitution than the normal lattice vibrations.) The optical transitions of the 3.188-eV center, unlike the 2.156-eV center, are virtually unaffected by uniaxial stress.[12] The lack of stress dependence explains why the spectrum of this center is considerably sharper than the spectrum of the 2.156-eV center. The lack of stress dependence, as well as the presence of high-frequency local modes in the vibronic spectrum,[18] strongly suggests that an interstitial atom is involved in this center. While the point-group symmetry of the center is not yet known, two models of the atomic structure have been proposed: an interstitial nitrogen atom,[12] and a substitutional nitrogen atom adjacent to a carbon interstitial.[18]

The dependence of the intensity of the 3.188-eV CL, feature (d), on electron-beam irradiation is not yet understood. Because the electron-beam energy of 10–30 keV is too low for primary radiation damage (the creation of a vacancy-interstitial pair in a perfect crystal), and because the 3.188-eV center is known to contain a nitrogen atom, it is clear that a precursor to center (d) must be present before irradiation; i.e., the role of the electron beam must be to induce a defect reaction. The simplest defect reaction would be the capture of one or more electrons, leading to a change in the charge state. We have not found a

similar report in the literature suggesting that irradiation by electrons in the keV range induces or enhances the 3.188-eV CL. There are, however, examples of similar behavior for other optical centers. For example, the 2.156-eV center is not observed immediately after primary radiation damage of a natural diamond crystal, but grows with time after the start of exposure to a keV-range electron beam;[14] the growth follows a saturating exponential curve.

Feature (e). The neutral atomic vacancy (GR center), a native defect produced by radiation damage in virtually all natural and synthetic diamonds,[4,5] has its principal zero-phonon line (the GR1 line) at 1.673 eV. Feature (e) has its peak at 1.675±0.002 eV; the small peak shift relative to the value reported for the GR center, as well as the large linewidth (0.025 eV), may arise from internal stress effects like those seen for the 2.156-eV center. Recently, we observed a similar component[22] in the laser photoluminescence (PL) spectrum in the same specimen (T_d=850 °C); the PL line has the same linewidth as the corresponding CL line, feature (e), but occurs at slightly higher energy, 1.680 eV; the energy difference between the PL and CL peaks is only 20% of the linewidth. Another luminescence line, at 1.685 eV, was first discovered in the CVD-grown epitaxial diamond-on-diamond films.[8] Subsequently, silicon ion-implantation experiments showed that the 1.685-eV line originates from a two–silicon-atom center.[23] More recent reports indicate that the silicon center has been observed in diamond films grown by microwave-plasma CVD, where the silicon atoms may originate from plasma etching of the silica walls of the reactor. There is thus a strong possibility of confusing the silicon center with the neutral vacancy in luminescence spectroscopy. The optical transitions of the silicon center are virtually unaffected by uniaxial stress,[8,23] a behavior similar to that of other interstitial-type defects. The luminescence line of the silicon center should therefore occur precisely at 1.685 eV and have a very narrow linewidth, even in specimens with large residual stress. For that reason, we attribute feature (e) in our specimens, as well as the similar photoluminescence line, to the neutral vacancy rather than the silicon center.

Of the five distinct CL centers that we have identified in our films, four were also observed in the homoepitaxial thermal-CVD-grown diamond films described in Ref. 8: the three nitrogen-related centers, features (a), (b), and (d), and the violet-emitting dislocation center, feature (c). The similar defect content of the polycrystalline and homoepitaxial films is noteworthy. Epitaxial diamond films, especially heteroepitaxial films which may become available in the future, are of interest for electronic and optoelectronic device applications, where optically and electrically active defects may either degrade or enhance device performance. CL in the films described in Ref. 9, grown by microwave-plasma-assisted CVD, consisted of band-A luminescence and possibly some dislocation-related violet luminescence [feature (c)]; none of the vibronic spectra of features (a), (b), (d), or (e) were observed in the latter films. CL imaging of these films showed that the CL arose from {100} faces, but not from {111} faces,[9] just as we observed for the dominant CL features (a) and (c) in the present study.

The presence of the 2.156-, 2.326-, and 3.188-eV nitrogen-related centers, features (a), (b), and (d), shows that nitrogen is readily incorporated into CVD diamond films. As the films were not intentionally nitrogen doped, the nitrogen must originate either from atmospheric contamination of the deposition system or from traces of nitrogen in the methane and hydrogen source gases. Atmospheric contamination is quite likely since the vacuum in the deposition chamber, maintained by a mechanical rotary pump, was no better than 20 Pa. Better control of the vacuum in the deposition chamber or of the purity of the source gases should make it possible to reduce the nitrogen content of the films.

The correlations between the intensity of the luminescence from various centers and the growth habit and morphology of the diamond films at different deposition temperatures are not understood at present. The following observations may, however, be made about the dislocation-related feature (c). The type of defect that gives rise to feature (c) is associated with {100} crystallographic faces (see Figs. 9 and 11). On the other hand, feature (c) is most intense in the specimens grown at T_d=700–800 °C, and particularly T_d=750 °C. These specimens have an octahedral growth habit and few {100} exterior faces. Other factors than crystallographic faces must therefore explain the high intensity of feature (c) in the 750-°C specimen. According to previous work, the dislocation-related violet CL is the dominant luminescence band in type-II*a* natural diamonds, which are relatively free of optically active defects and impurities. Further, the 750-°C specimen appears to have the most perfect crystalline microstructure of any of the CVD diamond specimens in the present study (see Fig. 8). It may be that the dislocation-related CL is quenched by competing trapping or recombination of carriers at other types of defects, which are present in higher concentration in the specimens grown at temperatures above or below 750 °C.

V. CONCLUSIONS

Cathodoluminescence imaging and spectroscopy in the SEM has been shown to be a useful tool for the study of defects in CVD-grown diamond films and particles. Several distinct types of CL centers have been identified in hot-filament CVD-grown diamond films. By making use of existing information about defect structures and spectra, we have shown that the CL centers are related to native defects, including atomic vacancies and dislocations, and to nitrogen impurity atoms. Changes in the intensity of the CL emitted by the various centers are strongly correlated with changes in morphology and crystal-growth habit as a function of deposition temperature. CL imaging has revealed that at least two centers, related to nitrogen-vacancy complexes and to dislocations, are primarily located in the near-surface regions adjacent to {100} crystal faces.

[1]A. Badzian *et al.*, in *Infrared and Optical Transmitting Materials,* edited by R. W. Schwartz (SPIE, Bellingham, WA, 1986) [Proc. SPIE **683**, 127 (1986)].
[2]R. C. DeVries, Annu. Rev. Mater. Sci. **17**, 161 (1987).
[3]V. K. Bazhenov, I. M. Vikulin, and A. G. Gontar, Fiz. Tekh. Poluprovodn. **19**, 1345 (1985) [Sov. Phys.—Semicond. **19**, 829 (1985)].
[4]C. D. Clark, E. W. J. Mitchell, and B. J. Parsons, in *The Properties of Diamond,* edited by J. E. Field (Academic, London, 1979), p. 23.
[5]J. Walker, Rep. Prog. Phys. **42**, 1605 (1979).
[6]B. G. Yacobi and D. B. Holt, J. Appl. Phys. **59**, R1 (1986).
[7]R. A. Roberts and W. C. Walker, Phys. Rev. **161**, 730 (1967).
[8]V. S. Vavilov *et al.*, Fiz. Tekh. Poluprovodn. **14**, 1811 (1980) [Sov. Phys.—Semicond. **14**, 1078 (1980)].
[9]H. Kawarada *et al.*, Jpn. J. Appl. Phys. **27**, L683 (1988).
[10]A. T. Collins and S. H. Robertson, J. Mater. Sci. Lett. **4**, 681 (1985).
[11]G. Davies, Rep. Prog. Phys. **44**, 787 (1981).
[12]A. M. Zaitsev, A. A. Gippius, and V. S. Vavilov, Fiz. Tekh. Poluprovodn. **16**, 397 (1982) [Sov. Phys.—Semicond. **16**, 252 (1982)].
[13]A. T. Collins, M. Stanley, and G. S. Woods, J. Phys. D **20**, 969 (1987).
[14]G. Davies, J. Phys. C **12**, 2551 (1979).
[15]K. Mohammed, G. Davies, and A. T. Collins, J. Phys. C **15**, 2779 (1982).
[16]N. Yamamoto, J. C. H. Spence, and D. Fathy, Philos. Mag. B **49**, 609 (1984).
[17]J. E. Ralph, Proc. Phys. Soc. London **76**, 688 (1960).
[18]A. T. Collins and G. S. Woods, J. Phys. C **20**, L797 (1987).
[19]A. T. Collins, G. Davies, H. Kanda, and G. S. Woods, J. Phys. C **21**, 1363 (1988).
[20]E. N. Farabaugh, A. Feldman, L. H. Robins, and E. S. Etz, in *Diamond Optics,* edited by A. Feldman and S. Holly (SPIE, Bellingham, WA, 1989) [Proc. SPIE **969**, 24 (1989)].
[21]J. C. Warmsley and A. R. Lang, J. Mater. Sci. Lett. **2**, 785 (1983).
[22]E. S. Etz, A. Feldman, L. H. Robins, and E. N. Farabaugh, in *Diamond Optics,* edited by A. Feldman and S. Holly (SPIE, Bellingham, WA, 1989) [Proc. SPIE **969**, 86 (1989)].
[23]A. M. Zaitsev, V. S. Vavilov, and A. A. Gippius, Kratkie Soobsh. Fiz. **10**, 20 (1981) [Sov. Phys. Leb. Inst. Rep. **10**, 15 (1981)].

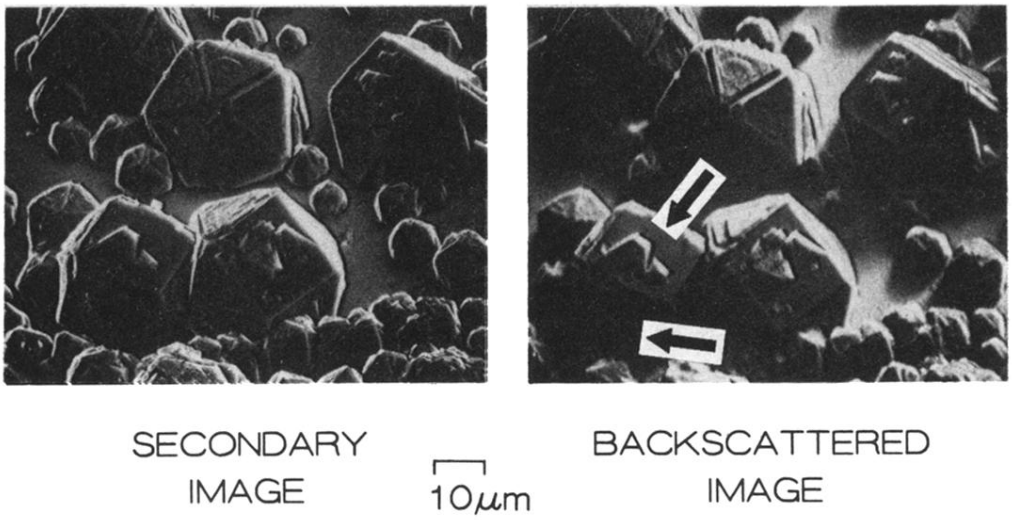

FIG. 10. Secondary-electron and backscattered-electron images of isolated particles; images of same spatial region as in Fig. 9; electron-beam energy is 20 keV.

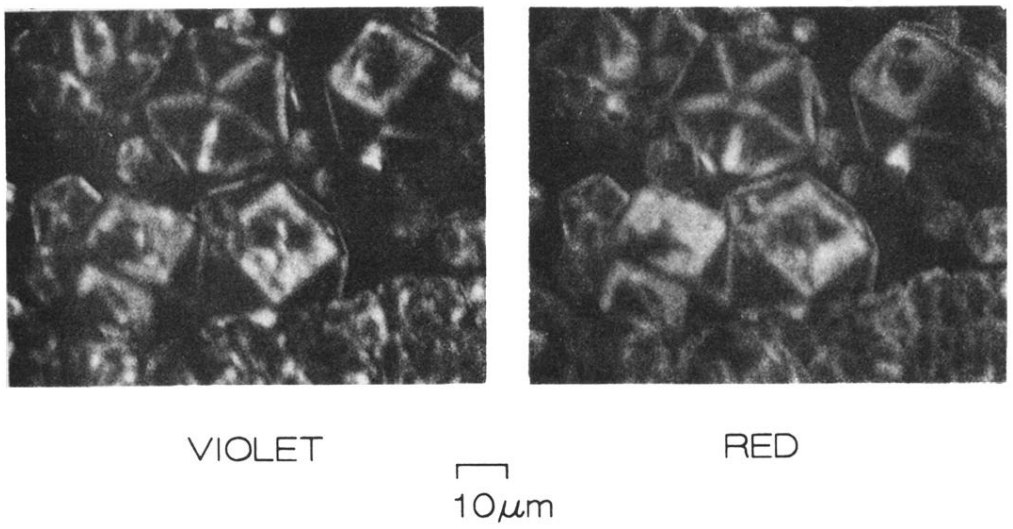

FIG. 11. Spectrally resolved CL images of isolated particles: broad violet component, 2.63–2.88 eV; broad red-to-yellow component, 1.85–1.97 eV; images of same spatial region as in Fig. 9; electron-beam energy is 20 keV.

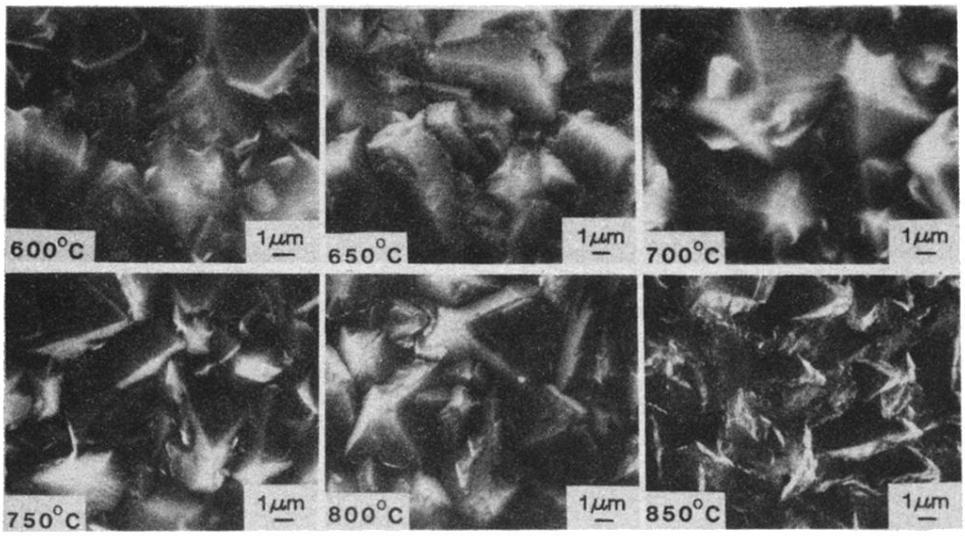

FIG. 8. Secondary-electron images of CVD diamond films, grown at six different deposition temperatures between 600 and 850 °C, obtained in scanning electron microscope at electron-beam energy of 20 keV.

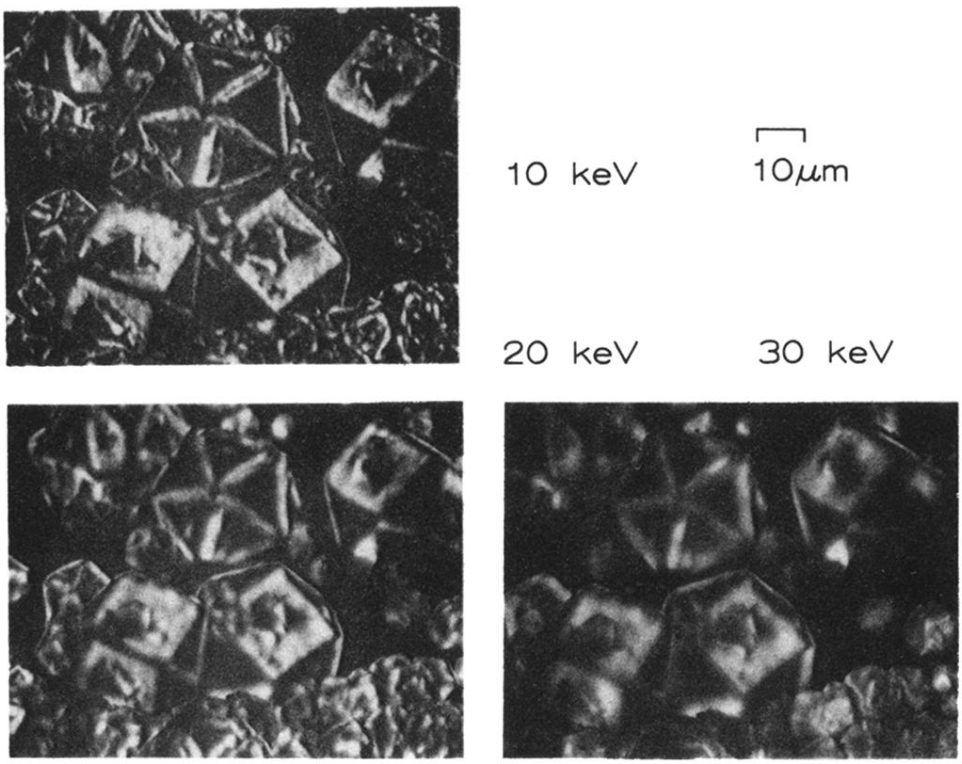

FIG. 9. CL images of isolated diamond particles, grown at 800 °C, obtained at electron-beam energies of 10, 20, and 30 keV.